6-2019

Case study on the effects of partial solar eclipse on distributed PV systems and management areas

Aditya Sundararajan

Temitayo O. Olowu

Longfei Wei

Shahinur Rahman

Arif I. Sarwat

IET Smart Grid

Case Study

IET Journals
The Institution of Engineering and Technology

Case study on the effects of partial solar eclipse on distributed PV systems and management areas

eISSN 2515-2947
Received on 4th January 2019
Revised 17th May 2019
Accepted on 20th May 2019
E-First on 20th June 2019
doi: 10.1049/iet-stg.2019.0002
www.ietdl.org

Aditya Sundararajan[1], Temitayo O. Olowu[1], Longfei Wei[1], Shahinur Rahman[1], Arif I. Sarwat[1] ✉

[1]*Department of Electrical and Computer Engineering, Florida International University, Miami, USA*

✉ *E-mail: asarwat@fiu.edu*

Abstract: Photovoltaic (PV) systems are weather-dependent. A solar eclipse causes significant changes in these parameters, thereby impacting PV generation profile, performance, and power quality of larger grid, where they connect to. This study presents a case study to evaluate the impacts of the solar eclipse of 21 August 2017, on two real-world grid-tied PV systems (1.4 MW and 355 kW) in Miami and Daytona, Florida, the feeders they are connected to, and the management areas they belong to. Four types of analyses are conducted to obtain a comprehensive picture of the impacts using 1 min PV generation data, hourly weather data, real feeder parameters, and daily reliability data. These analyses include: individual PV system performance measurement using power performance index; power quality analysis at the point of interconnection; a study on the operation of voltage regulating devices on the feeders during eclipse peak using an IEEE 8500 test case distribution feeder; and reliability study involving a multilayer perceptron framework for forecasting system reliability of the management areas. Results from this study provide a unique insight into how solar eclipses impact the behaviour of PV systems and the grid, which would be of concern to electric utilities in future high penetration scenarios.

Nomenclature

Systems

$\mathscr{A}$ 1.4 MW PV system located at Miami, FL
$\mathscr{B}$ 355 kW PV system located at Daytona, FL

Variables

$\%_{\text{temp\_coeff}}$	PV module's rated temperature coefficient
D	net derate factor of the PV system
E_{estimate}	expected energy from PV system for a year
$I_{n,\text{ RMS}}$	RMS magnitude current of the nth harmonic
$\text{Ir}(t)$	irradiance measured in W/m^2 at the time t
$\text{kWAC}_{\text{actual}}(t)$	power generated by the PV system at the time t
$\text{kWhAC}_{\text{actual}}$	energy produced by the PV system as observed (kWh)
$N_{\text{CapSwitching},\,t}$	number of switching operations at the time t
$N^{\text{max}}_{\text{CapSwitching}}$	maximum total number of capacitor switching operations per day
$N_{\text{DailyCapSwitching}}$	maximum allowable number of tap changes
$N_{\text{max}-\text{tap},\,t}$	maximum allowable number of tap changes
$N_{\text{taps},\,t}$	number of tap changes made by the LTCs at time t
P_{L}	load active power
p_{cable}	derate factor capturing cable losses
P_{DC}	nameplate capacity of the PV system
p_{dirt}	derate coefficient representing dirt
$P_{\text{estimate}}(t)$	expected power from PV system at the time t
p_{inverter}	derate factor capturing inverter's conversion loss, also called efficiency
P_{lt}	long-term flicker
p_{mismatch}	PV module mismatch coefficient $= \dfrac{P_{\text{panel}} - P_{\text{MPP}}}{P_{\text{MPP}}}$
p_{MPP}	maximum power point wattage of the PV module (W)
p_{panel}	maximum wattage of the PV module (W)
P_{PV}	injected active power
P_{st}	short-term flicker
$\text{PPI}(t)$	power performance index of the PV system at the time t
Q_{L}	load reactive power
Q_{base}	base voltage at POI
Q_{cb}	reactive power injection by capacitor banks
Q_{PV}	injected reactive power
R	feeder resistance
t	time-step instance
$T(t)$	PV module's temperature at the time t
$T_{\text{cell\_avg}}$	average temperature of a PV cell (°C)
Tap_t	tap position of the LTCs at time t
$V_{n,\,t}$	actual bus voltage at time t
V_n^{max}	maximum allowable node voltage
V_n^{min}	minimum allowable node voltage
X	feeder reactance
$X_{n,\text{ RMS}}$	RMS magnitude (either voltage or current) of the nth harmonic
$X_{o,\text{ RMS}}$	RMS magnitude (either voltage or current) of the fundamental frequency

1 Introduction

Power generation from renewable energy sources (RESs) has become inevitable owing to the environmental impacts of generating power from conventional sources such as coal. However, the generation from RESs such as photovoltaic (PV) systems is dependent on several external parameters — solar irradiance, ambient temperature, module temperature, wind velocity (wind speed and direction), dust, cloud cover (cloud coverage area, cloud density, and cloud velocity), soiling, and shading [1, 2]. Some intrinsic parameters such as conversion losses and cabling losses, which can be summarised as derate factors, also influence the net output from PV systems. However, the most dominant of these factors are the irradiance, ambient temperature, and module temperature [3]. One event that alters these parameters over a very short duration, thereby impacting PV generation, is the solar eclipse.

A solar eclipse occurs whenever the moon passes between the Sun and the earth, blocking the path of the solar radiation to the earth. The moon is capable of entirely blocking out the Sun since

the ratio of the diameter to the distance from the earth for both the moon and the Sun is the same. A total eclipse occurs when the moon blocks the Sun entirely, and partial otherwise. There are other types of solar eclipses too, but their discussion is beyond the scope of this paper. While a solar eclipse is accurately predictable, its impact on the smart grid has been less emphasised in the literature.

Utilities conduct pre-eclipse studies using spatial and temporal profiling to regularly monitor the generation profiles of PV and profiles of connected loads. This helps system planners better to schedule and allocate their resources to cope with the impending impact of the eclipse. Prior to the North American 21 August 2017 eclipse, a combined loss of 3.5 GW in utility scale, 1. 5GW loss in rooftop PV power generation in California, and a total loss of 5.2 GW in the whole of the United States were projected [4, 5]. On the basis of weather prediction and the projected loss of generation, many other conventional generation sources and energy storage are dispatched to compensate for the loss in the generation and the change in load during the eclipse [6]. This in-depth pre-event analysis is, however, largely restricted to utility-scale PV systems, because there is little operational visibility on distributed PV such as rooftop solar and small commercial systems at offices, universities, and buildings [7]. Although not of concern now, the dynamics will change when the penetration level (the volume of PV-connected relative to the amount of load) of such distributed PV systems increases drastically, wherein grid operations will be significantly impacted [8, 9]. The steep ramp rates due to the loss of generation and the possible change in load patterns due to the eclipse could potentially impact the stability of the system. Hence, there is a need to evaluate the impacts of the solar eclipse on distributed PV systems to provide a roadmap for the utilities to prepare for eclipses in the future.

To, this effect, this paper explores the impacts of the eclipse of 21 August 2017 on two distributed PV systems from an individual system-level up to the management-area level. The presented case study considers systems located in Florida with different generation nameplate capacities: 1.4 MW (system $\mathscr{A}$ at Miami) and 355 kW (system $\mathscr{B}$ at Daytona). The study is divided into four analyses during the eclipse peak: performance measurement and relationship analysis for the systems, power quality analysis at the point of interconnection (POI) of system $\mathscr{A}$, simulation of voltage device operations on an IEEE 8500 test case distribution feeder network remodelled to include real system parameters of the feeders that the two PV systems connect to, and finally, system reliability evaluation and forecasting for the utility management areas (Miami and Daytona). Different datasets are used for conducting these analyses after being subject to quality checks [10, 11]: real-time-series PV generation data of 1 min resolution collected from cloud-based on-site data acquisition systems (DASs) for system performance; real-time-series average root-mean-square (RMS) voltage, harmonics (voltage, current), and instantaneous flicker (IFL), short-term flicker (P_{st}), and long-term flicker (P_{lt}) data of 1 min resolution collected from the POI of system $\mathscr{A}$ using a metre for power quality analysis; smart inverter data sheets (for power-efficiency curves), PV data sheets (for temperature-efficiency curve), and load profile data for the voltage profile analysis; moreover, hourly weather data from the National Climatic Data Centre and daily reliability data for the two management areas for the reliability analysis.

The key contributions of this paper are that it: (i) investigates events such as solar eclipse that have short term, but high-magnitude impacts on PV generation unlike a majority of the literature that deals with fluctuations over longer periods of time (Sections 2 and 3); (ii) analyses the impacts of solar eclipse on PV systems: performance (Section 4.1), power quality at POI (Section 4.2), voltage profiles of feeders (Section 4.3), and reliability of management areas (Section 4.4); (iii) provides a roadmap for utility distribution planners to better handle the impacts of solar eclipses under future high PV penetration scenarios (Section 4); (iv) proposes power performance index (PPI), an effective metric, to quantify instantaneous PV performance during the eclipse peak that can be used by utilities in planning studies (Section 5.1); (v) quantifies power quality parameters and measures deviations from the standard values during the eclipse at existing and future high penetration scenarios to help utilities take some proactive steps to mitigate the possible power quality violations that could arise as a consequence of the eclipse event. (Section 5.2); (vi) quantifies the eclipse's impact on voltage regulating devices using real system parameters to enable utility companies take proactive voltage control steps through the use of smart inverter settings and optimal coordination of other voltage regulating devices in the network (Section 5.3); and (vii) develops regression models to analyse the relationship between weather parameters and reliability indices of management areas and forecast the indices, thereby helping utilities evaluate how solar eclipses impact the stability of the grid at a larger scale (Section 5.4). Finally, Section 6 concludes the study and provides future directions for research in the area.

2 Related work

Studies have been conducted to determine the overall behaviour of PV systems during an eclipse. A study monitored the performance of a 4.85 kW PV system during the 21 August 2017 eclipse and estimated the performance measurements using irradiance calculation approaches [12]. However, it does not quantify the performance of the system using one of the standard accepted metrics such as performance ratio (PR), energy performance index, or PPI as recognised by the industry [13–16]. A similar study of PV performance was conducted by other authors too, but they primarily relied on comparing the net PV generation on the day of the eclipse versus the following: generation of the same system on the same date of the previous year or generation of the same system on the date prior to or next to the date of the eclipse [17, 18]. While these methods provide a visual idea about the impact of the eclipse, they do not quantify the impacts as a measurable metric. Furthermore, these studies limit their scope to a single system of concern, thus not considering potential understandings of how an eclipse could impact PV over a larger area and what that might mean for aggregation-related studies in the future. The performance metrics defined in Section 4.1 are derived from industry-accepted metrics that have recently gone beyond the traditionally used PR [14, 19]. Kumar and Sudhakar [20] evaluated different metrics for PV performance, but it considers metrics which have certain limitations. For example, it looks at yield and capacity factor which depend on the PV system nameplate capacity, PR which depends on the PV system model and the local weather parameters, not consider PPI which is a more effective metric to compare performances of systems of different sizes, and system generation which is not a direct measure of performance.

Many research papers have studied the technical limitations and unfavourable effects on power quality such as feeder voltage variations, small range voltage fluctuations, and harmonic injections on power system parameters resulting from intermittent PV generation [21, 22]. None of them, however, focus on special events such as a solar eclipse. Voltage sag, swell, and small range voltage fluctuations are very common and could have been observed at the POI during [23]. The semiconductor devices used in inverter-based PV systems inject significant harmonics and could increase the power losses on the grid [24]. It is necessary to investigate the effects of grid-tied PV system due to different weather related events such as solar eclipse for reliable and continuous power supply. The extent of power quality impact depends on network configuration, weather variability, and the location of the PV plant. The power quality analyses were carried out on system $\mathscr{A}$ at Miami.

The integration of PV systems on distribution feeders (depending on their locations) usually have some impacts on the operations on the voltage regulating devices such as voltage regulators (VRs), on/off load tap changers (OLTCs), capacitor banks, and VRs [25]. These impacts are usually observed in terms of the number of switching operations of these devices. Owing to PV integration, there could be an increase or decrease in the number of switching of these devices depending on the feeder profile, the location of the PV, and the operation of the smart inverters. The life span of these devices usually is impacted by the number of their switching operations. This could attract some huge

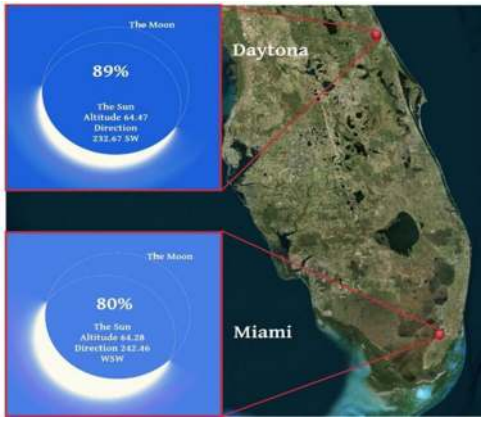

Fig. 1 *Statistics of the partial solar eclipse at the two locations*

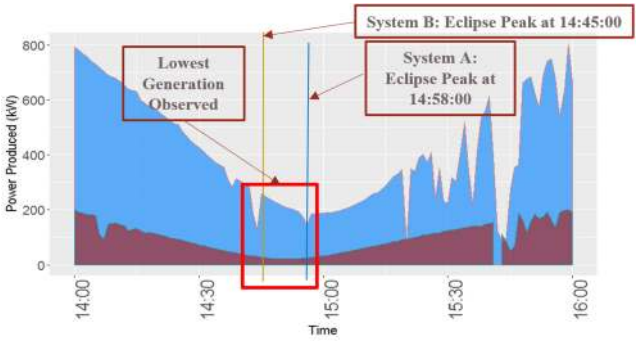

Fig. 2 *TDD during solar eclipse period*

Table 1 Statistics about the partial solar eclipse

Value (from 2 to 3 PM)	System $\mathscr{A}$	System $\mathscr{B}$
location	Miami	Daytona
time at the lowest reading	3:00 PM	2:45 PM
drop in power, kW	503.4 (70.8%)	140.64 (84%)
drop in irradiance, W/m^2	469.99 (70.8%)	56.3 (87.4%)
drop in ambient temperature, F	3.48 (3.8%)	6.92 (7.4%)
drop in module temperature, F	13.52 (13.1%)	25.4 (21.8%)
change in PPI	1.5%	0.3%

financial cost for utility companies due to the possible need to maintain of totally replacing these devices. Most studies reported on the impact of the eclipse events did now show their impacts on these voltage regulating devices [26, 27]. Usually, these switchings are difficult to capture on a live distribution system during their operations. The planning departments of many utility companies, therefore, simulate these events for a study-impact analysis which is usually not made public.

Severe weather conditions such as typhoons, ice storms, and earthquakes have recently been considered to study the power system reliability performance [28–30]. In [28], the effects of different types of severe weather conditions on the reliability performance of power system components were evaluated, and the existing methodologies for modelling these effects were listed and compared. A reliability assessment framework was proposed in [29] for quantifying the power transmission system performance under the typhoon weather. In [30], a defensive islanding-based operational enhancement approach was developed to improve the power system resilience to extreme weather events. This is in contrast with the solar eclipse that only involves predictable changes in common weather parameters such as temperature and solar radiation. Hence, the required methods of analyses are applicable more for analysing system reliability under common weather conditions, not extreme. In [31], a power distribution system reliability assessment framework was presented using time-series common weather data. A statistical model was introduced in [32] to predict the daily number of common weather-based power interruptions in power distribution systems, but there is a lack of literature which explores system reliability during eclipses.

3 Background for the case study

This section provides a brief background for the case study including some information on the 21 August 2017 eclipse.

3.1 Eclipse of 21 August 2017

The total solar eclipse of 21 August 2017 was the first to be observed in 26 years from the USA. It was first observed in Oregon at 10:15 AM (Pacific Time) and last observed in North Carolina at 2:49 PM (Eastern Time). During the short period of the eclipse at each location, the utilities were reported to have taken their PV systems offline, wherein a surge in load was also expected. In the state of Florida, the eclipse was only partial. The two utility management areas considered in this paper, Miami and Daytona, experienced an average coverage of about 80 and 89%, respectively, as illustrated in Figs. 1 and 2. As noted in Section 1, the two systems, the feeder model, and the management areas considered for the case study are described in the following sections.

3.2 Two grid-tied PV systems $\mathscr{A}$ and $\mathscr{B}$

Table 1 summarises the key changes observed in a net generation, average irradiance, average temperature, and average PPI of the two PV systems under consideration. It can be observed that system $\mathscr{B}$, for reasons described in Section 3.2, experienced a greater fluctuation in module temperature, ambient temperature, and irradiance, but recorded a lower fluctuation in its instantaneous performance which is measured using the PPI. This metric is discussed in detail in Section 4.1.

The two PV systems deploy different smart inverter topologies. While system $\mathscr{A}$ uses string inverters and a cluster controller to aggregate individual inverter productions, system $\mathscr{B}$ uses a combination of micro-inverters and string inverters [33]. Locally installed weather stations measure global horizontal irradiance, module temperature, and ambient temperature with up to a resolution of 1 min. A cloud-based DAS is used to access the raw data for further processing and analysis, as described in [34, 35]. Systems $\mathscr{A}$ and $\mathscr{B}$ are connected to feeders $\mathscr{A}$ and $\mathscr{B}$, respectively, which are radially distributed from their substations located in Miami and Daytona, respectively.

3.3 IEEE 8500 test feeder for systems $\mathscr{A}$ and $\mathscr{B}$

The standard IEEE 8500 test network was developed from a real distribution feeder in the USA. The feeder has both the medium- and low-voltage levels with the longest node being ∼17 km from the substation (Fig. 3). It has four capacitor banks (three controlled and one fixed), three VRs with tap-changeable substation transformer. The feeder model also contains both balanced and unbalanced loads [36]. For this simulation, the line characteristics and load profiles of the feeders $\mathscr{A}$ and $\mathscr{B}$ were used to modify the standard IEEE test feeder. The two PV systems ($\mathscr{A}$ − and $\mathscr{B}$) were modelled using OpenDSS and subsequently integrated into the test feeder. The irradiance and temperature profiles during the eclipse were also used for the PV systems modelling. The penetration level of the PV on this feeder is ∼37%, which is defined as the ratio of the PV-installed nameplate capacity to the total size of the loads on the feeder.

3.4 Management areas comprising systems $\mathscr{A}$ and $\mathscr{B}$

The Systems $\mathscr{A}$ and $\mathscr{B}$ are, respectively, located at the Miami and Daytona management areas. For these two areas, the reliability indices collected contain the sustained and momentary interruption events: system average interruption duration index, customer average interruption duration index, system average interruption frequency index, CAIFI, and momentary average interruption frequency index. The numbers of sustained and momentary interruption events play a key point in reliability analysis, and other

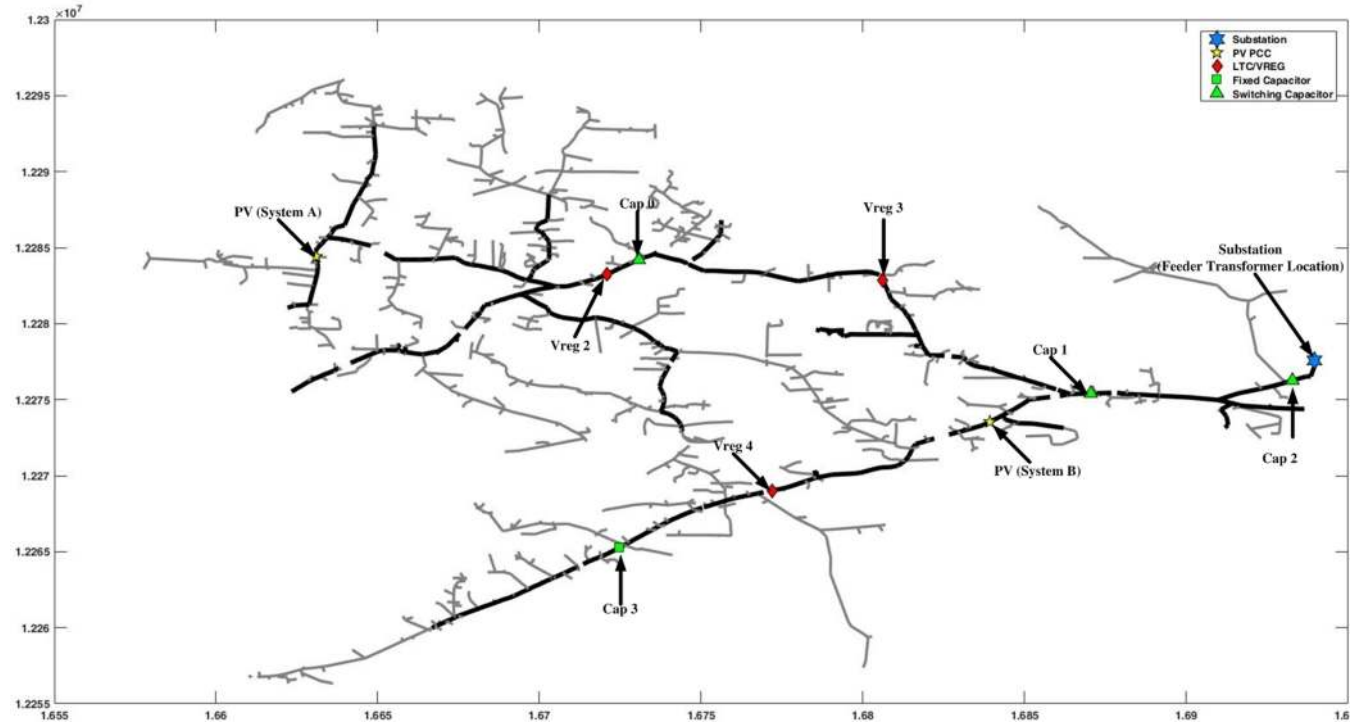

Fig. 3 *IEEE 8500 test feeder with the integration of PVs (systems $\mathscr{A}$ and $\mathscr{B}$)*

Table 2 Power and energy estimation parameters for $\mathscr{A}$ and $\mathscr{B}$

Parameter	System $\mathscr{A}$	System $\mathscr{B}$
p_{dirt}	0.9	0.9
p_{mismatch}	0.97	0.97
p_{cable}	0.99	0.99
p_{inverter}	0.98	0.9725
$\%_{\text{temp\_coeff}}$	−0.5	−0.5

reliability metrics can be calculated based on these values. Therefore, the sustained and momentary interruption events happening during the solar eclipse are selected for reliability analysis. The common weather parameters such as temperature, precipitation, air pressure, and wind speed are mainly collected from the Miami and Daytona International Airports. Additionally, the lightning data are provided by the control centre of the local electric utility, which installs its own weather stations in its different management areas.

4 Model formulation

This section describes in detail the different methods used to evaluate system performance, power quality at the POI, voltage device operations at the feeders, and management-area reliability.

4.1 PV system performance

Many metrics are currently used to evaluate PV system performance [37–40]. PR is a widely used metric, defined as the ratio of observed power (over short durations from minutes to a day) or energy (over the long duration from months to a year) to the expected power or energy, respectively. Given P_{DC}, $\text{Ir}(t)$, and the irradiance measured at standard test conditions (STCs) $\left(1000\,\text{W/m}^2\right)$, the values of $P_{\text{estimate}}(t)$ and E_{estimate} are calculated using (1), considering 1 min resolution data [37]

$$\begin{aligned} P_{\text{estimate}}(t) &= P_{\text{DC}} \times \frac{\text{Ir}(t)}{1000} \times X \times D \\ E_{\text{estimate}} &= P_{\text{DC}} \times X \times D \times \sum_{i=1}^{525,\,600} \frac{\text{Ir}(t)}{1000} \end{aligned} \tag{1}$$

where D is a function of p_{dirt}, p_{mismatch}, p_{cable}, and p_{inverter} such that [41, 42]

$$D = p_{\text{dirt}} \times p_{\text{mismatch}} \times p_{\text{cable}} \times p_{\text{inverter}} \tag{2}$$

The variable X in (1) can be modified to improve the accuracy of the estimation and takes two parameters into account: $T(t)$ and $\%_{\text{temp\_coeff}}$. When $X = 1$, it is called *uncorrected estimation*, and when $X = 1 + \frac{\%_{\text{temp\_coeff}}}{100}[T(t) - 25]$, the estimation considers the effect of $T(t)$ by correcting it to the STC ($25°C$). It has been shown that the accuracy of estimation is maximised when $T(t)$ is corrected instead to $T_{\text{cell\_avg}}$ and wind speed [43]. In this paper, $T(t)$ is corrected just to $T_{\text{cell\_avg}}$, with all 1 min data points averaged over a period from 01 January through 31 December 2017, for the study (Table 2).

PR, measured using (3) [39, 40], is widely used by the utilities to measure the performance of a particular PV system; it has some key demerits [44]: (i) highly dependent on local weather (especially module temperature) and hence varies significantly over the course of a year and (ii) varies depending on the nameplate capacity of the system. Owing to these reasons, PR is not an effective metric to compare the performance of any two given PV systems

$$\text{PR} = \frac{\text{kWhAC}_{\text{actual}}}{P_{\text{DC}}} \times \frac{1000}{\sum_t \text{Ir}(t)} \tag{3}$$

There exist other metrics such as yield (PV systems of different sizes are not directly comparable) and PR corrected to $T(t)$ and wind speed (PV systems employing different PV models are not directly comparable). A new metric called the PPI is used in this paper, which is calculated as [45]

$$\text{PPI}(t) = \frac{\text{kWAC}_{\text{actual}}(t)}{P_{\text{estimate}}(t)} \tag{4}$$

PPI is better to compare the performance of different PV systems because: (i) it corrects the estimation to average module temperature to account for local variations and (ii) it is independent of the inherent PV model. There exists the energy performance index too, but it is used for comparing the performance of PV systems over an aggregated period of time. Since the eclipse lasts for a shorter period and its impacts should be evaluated over a short duration, PPI emerges as a better metric overall.

4.2 Power quality analysis at the POI

Integration of inverter-based PV system into the grid introduces non-sinusoidal waveforms that degrade power quality at the POI. Indices such as average RMS voltage, total harmonic distortion (THD) of voltage and current, total demand distortion (TDD), and flicker – IFL, P_{st}, and P_{lt} – are used to quantify the quality of power. Several standards such as IEEE Standard 1547-2018 (voltage regulation), IEEE Standard 519-2014 (harmonics regulation), and IEEE Standard 1453-2015 (flicker regulation) provide a set of criteria and requirements for the interconnection of RESs into the power grid and help in quantifying deviations from the ideal values.

PV integration could lead to changes in feeder voltage as well as the line loading. The voltage change at the POI can be expressed as follows [46]:

$$\Delta V = \frac{R(P_{\mathrm{L}} - P_{\mathrm{PV}}) + X(Q_{\mathrm{L}} - Q_{\mathrm{PV}})}{V_{\mathrm{base}}} \tag{5}$$

THD is a comparison of total harmonic content in a voltage or current waveform to the 60 Hz fundamental magnitude that is expressed in (6) [47]. Typical voltage THD level varies between 0.5 and 5%, and current THD ranges from 0.5 to 80% or more, depending on the type of load, amount of PV generation, PV penetration level etc.

$$\mathrm{THD} = \frac{\sqrt{\sum_{n=2}^{\infty} X_{n,\,\mathrm{RMS}}^2}}{X_{o,\,\mathrm{RMS}}} \times 100\% \tag{6}$$

where X_{fundRMS} and $X_{n\mathrm{RMS}}$ are the RMS magnitude (either voltage or current) of the fundamental frequency and nth harmonic, respectively.

Current THD depends on the change of the RMS current magnitude without considering load types (harmonic or non-harmonic loads). Switching ON/OFF a linear load causes significant changes in RMS current and current THD, even if the load does not produce any harmonics. TDD is an appropriate term to analyse harmonics in voltage or current waveforms, which compares the root-sum-square value of the harmonic current to the maximum demand load current as represented by (8) [47]. Changes in non-harmonic loads do not cause any change in TDD as it is a normalised value

$$\mathrm{TDD} = \frac{\sqrt{\sum_{n=2}^{\infty} I_{n\mathrm{RMS}}^2}}{\text{maximum demand load current}} \times 100\% \tag{7}$$

Flicker measures the level of small voltage fluctuations and expresses the reaction of the human eye in response to a light source. IFL quantifies a sudden voltage change. Events that cause a dip in the voltage magnitude immediately interrupts the IFL data. Cumulative weighted probability of flicker perception levels at 0.1, 1, 3, 10, and 50% of each 10 min time period determine the value of P_{st}, which is expressed in the equation below [48]:

$$P_{\mathrm{st}} = \sqrt{0.0314P_{0.1} + 0.0525P_1 + 0.0657P_3 + 0.28P_{10} + 0.08P_{50}} \tag{8}$$

where $P_{0.1}$, P_1, P_3, ... denote the ratio of voltage magnitude change ($\Delta V = V_{\max} - V_{\min}$) to the base voltage ($V_{\mathrm{base}}$). An average of P_{st} over 2 h defines P_{lt}, which is expressed in the equation below [48]:

$$P_{\mathrm{lt}} = \sqrt[3]{\frac{1}{12}\sum_{i=1}^{12} P_{\mathrm{st}}^3} \tag{9}$$

4.3 Voltage device operation analysis at the feeders

Integration of PV systems on distribution feeders has some potential impacts on the operation of the legacy devices (VRs, capacitor banks, reactors, and LTCs) in the network [49, 50]. For most traditional grid systems, utility companies often use OLTCs and regulators for voltage regulation on their distribution feeders. Switched capacitor banks are used for reactive power compensation which consequently affects the voltage profile of the feeder. More recently, the use of smart inverters for voltage regulation and optimisation has become a viable option. The major concerns with the use of VRs and OLTCs are the number of switching operations being carried out by these devices. The life span of VRs and OLTCs are directly impacted by the number of switching operations per day. According to [51, 52], a high-quality VR is capable of making 2 million mechanical switchings (273 switching operations per day) without the need for maintenance over a 20 year life span.

Most commercially available OLTCs and VRs typically have a total of 32 steps with a 0.625% change in voltage with each tap step. For VRs and LTCs, the turns ratio must satisfy the constraint expressed in the equation below [49]:

$$\mathrm{Tap}_{\mathrm{high}} \geq \mathrm{Tap}_t \geq \mathrm{Tap}_{\mathrm{low}} \tag{10}$$

To better restrict the number of switching operations of the tap changers for optimal operations and simulation studies, the number of switching operations of the LTC within a time interval t to T should satisfy the equation below [49]:

$$\sum_{t=1}^{T} N_{\mathrm{taps},\,t} \leq N_{\mathrm{max-tap},\,t} \tag{11}$$

where $N_{\mathrm{taps},\,t}$ is the number of tap changes made by the LTCs and $N_{\mathrm{max-tap},\,t}$ is the maximum allowable number of tap changes.

The impact of the eclipse on the switching of the capacitor banks can also be quantified within the period of interest. Capacitor bank switching constraints and reactive power injection is as given in (12) and (13), respectively [49, 50]

$$N_{\mathrm{DailyCapSwitching}} = \sum_{t=1}^{T} N_{\mathrm{CapSwitching},\,t} \leq N_{\mathrm{CapSwitching}}^{\max} \tag{12}$$

$$|Q_{cb\max}^{n}| \geq |Q_{cb}^{n}| \tag{13}$$

where $N_{\mathrm{Daily\,Cap\,Switching}}$ is the total number of switching steps by the switched capacitor in a day, $N_{\mathrm{Cap\,Switching},\,t}$ is the number of switching operations at a time interval t, $N_{\mathrm{Cap\,Switching}}^{\max}$ is the maximum total number of capacitor switching operations per day, $Q_{\mathrm{cb\,max}}^{n}$ is the maximum allowable reactive power injection by a capacitor bank and Q_{cb}^{n} is the actual reactive power injection by the capacitor bank.

The bus voltages at each node should also be within the ANSI C84.1-2011 [50]

$$\begin{gathered} V_n^{\max} \geq V_{n,\,t} \geq V_n^{\min} \\ 1.05\ \mathrm{pu} \geq V_{n,\,t} \geq 0.95\ \mathrm{pu} \end{gathered} \tag{14}$$

where $V_n^{\max}$ is the maximum allowable node voltage (1.05 pu), $V_{n,\,t}$ is the actual bus voltage at the time t, and $V_n^{\min}$ is the minimum bus voltage (0.95 pu).

4.4 Reliability analysis at the management areas

The solar eclipse is usually accompanied by multiple common weather changes such as temperature and air pressure changes and a loss in solar irradiation. Here, the regression analysis is implemented to model the reliability metrics of the Miami and Daytona management areas under common weather conditions. Given a time period T, $\boldsymbol{N} = (n_1, \ldots, n_T)$ is defined to be the daily reliability metric vector (for example, sustainable interruption), and $\boldsymbol{X} = (x_1, \ldots, x_T)$ represents a common weather parameter vector. The relationship between $\boldsymbol{N}$ and $\boldsymbol{X}$ then can be mathematically defined as: $\boldsymbol{N} = f(\boldsymbol{X}, \boldsymbol{\beta}) + \boldsymbol{\varepsilon}$, where $f(\cdot)$ denotes the regression function, typically polynomial, and exponential functions [53]; $\boldsymbol{\beta}$ represents the estimation parameter vector; and $\boldsymbol{\varepsilon}$ indicates a zero-sum white Gaussian noise. In this paper, we mainly consider five main weather parameters including the average temperature T, the sustained wind speed W, the daily rain precipitation P, the average air pressure A, and the daily number of lightning strikes L. Taking the daily number of sustainable interruptions from 1 January 2015 to 30 April 2017 as $\boldsymbol{N}$, the relationship function between $\boldsymbol{N}$ and each weather parameter can be calculated as [54]

$$\begin{aligned} N_{\mathrm{T}} &= \beta_0^{\mathrm{T}} + \beta_1^{\mathrm{T}} T + \beta_2^{\mathrm{T}} T^2 + \beta_3^{\mathrm{T}} T^3 \\ N_{\mathrm{W}} &= \beta_0^{\mathrm{W}} + \beta_1^{\mathrm{W}} \exp(\beta_2^{\mathrm{W}} W) + \beta_3^{\mathrm{W}} \exp(\beta_4^{\mathrm{W}} W) \\ N_{\mathrm{P}} &= \beta_0^{\mathrm{P}} + \beta_1^{\mathrm{P}} \exp(\beta_2^{\mathrm{P}} P) + \beta_3^{\mathrm{P}} \exp(\beta_4^{\mathrm{P}} P) \\ N_{\mathrm{A}} &= \beta_0^{\mathrm{A}} + \beta_1^{\mathrm{A}} A + \beta_2^{\mathrm{A}} A^2 + \beta_3^{\mathrm{A}} A^3 \\ N_{\mathrm{L}} &= \beta_0^{\mathrm{L}} + \beta_1^{\mathrm{L}} L + \beta_2^{\mathrm{L}} L^2 + \beta_3^{\mathrm{L}} L^3 \end{aligned} \tag{15}$$

where, for T, A, and L, the relationship function is represented as a polynomial regression function with third degree, while, for W and P, the relationship function is represented as the exponential regression function with two terms.

Taking the common weather parameters T, W, P, A and L, and their corresponding regression results N_{T}, N_{W}, N_{P}, N_{A}, and N_{L} derived by (15) as inputs, multilayer perceptron (MLP) is developed for forecasting the daily number of sustainable interruptions N. The MLP is a feed-forward neural network containing the input, hidden, and output layers [55]. The proposed MLP model consists of the 10 features mentioned earlier in the input layer ($\ell = 1$), one hidden layer with five units, and an output layer N_{pre} ($\ell = 3$) with 1 unit. All the weights $\left(w_{ji}^{\langle l \rangle}\right)$ between layers $\ell = 1$ and $\ell = 3$ are initialised to a set of sample values that are drawn from specific distributions instead of being randomly initialised. To achieve faster convergence and avoid saturation of activation functions during training, this paper uses Xavier uniform [56] and uniform distributions [57] to initialise the weights of MLP. To minimise the loss function [mean-square error (MSE)] between predicted and actual outputs during testing and training, backpropagation (BP) is used. In the input layer, the MLP neurones receive the common weather parameters and their regression results for analysis. The neurones of the output layer provide the network results for the daily number of sustainable interruptions. In the hidden layer, the MLP neurones represent the relationship between the inputs and outputs in the network. In addition, all MLP neurones are implemented with non-linear activation functions (sigmoid and hyperbolic tangent [58]) and each MLP layer is fully connected to the next layer without the use of dropout regularisation. The mathematical expression of the outputs of the MLP can be defined as [54]

$$N = F\left(b + \sum_{j=1}^{m} v_j \left[\sum_{i=1}^{n} G\left(w_{ij} x_i + b_j\right)\right]\right) \tag{16}$$

where $(x_1, \ldots, x_n)$ denotes the input vector including T, W, P, A, L, N_{T}, N_{W}, N_{P}, N_{A}, and N_{L}; N represents the output value; w_{ij}, $j = 1, \ldots, m$, is the weight of connection between the ith input neurone and the jth hidden neurone; v_j is the weight of connection between the jth hidden neurone and output neurone; b and b_j are the bias values of the corresponding output neurone and the jth hidden neurone; and $F(\cdot)$, $G(\cdot)$ are the activation functions of output and hidden neurones, respectively. An MLP architecture can contain more than one hidden layers between the input and output layers. In this paper, to restrict the net capacity, one hidden layer is included in the MLP, and BP algorithm [59] is used to train the MLP architecture parameters including w_{ij}, v_{ij}, b, and b_j, where $i = 1, \ldots, n$ and $j = 1, \ldots, m$.

Table 3 PPI for systems $\mathscr{A}$ and $\mathscr{B}$

Time, PM	System $\mathscr{A}$	System $\mathscr{B}$
2:44	1.071	9.975
2:45	1.103	**10.018**
2:46	1.107	**10.319**
2:47	1.101	9.452
2:57	1.084	9.676
2:58	**1.082**	9.447
2:59	**1.091**	9.629
3:00	1.091	9.885

The bold values show the peaks of the solar eclipse at the locations of systems A and B and their respective PPIs.

5 Case study results

This section discusses the results derived from applying the formulated models to the systems of concern.

5.1 PV system performance

Table 3 shows the PPI for systems $\mathscr{A}$ and $\mathscr{B}$ during the peak of the eclipse. During the respective moments of eclipse peak (2:58 PM for system $\mathscr{A}$ and 2:45 PM for system $\mathscr{B}$), the PPI increases, which is reflected in the values recorded at the next minute (2:59 PM for system $\mathscr{A}$ and 2:46 PM for system $\mathscr{B}$). Following from (4), in ideal cases, the value of PPI must be close to unity because it is the ratio of observed to the expected power at a given point in time. However, the reality could be quite different, given the influence of different external factors and errors in data acquisition. These factors might cause the expected generation to exceed or fall short of the actual generation, thereby tipping the ratio to be less than unity or greater than unity, respectively. By observing the PPI values for the two systems, it can be concluded that the values of PPI are close to unity for system $\mathscr{A}$, implying that the estimation model shows good performance. However, the PPI values of system $\mathscr{B}$ exceed unity, implying the estimated values are lower than the observed values. Investigating the factors influencing the poor performance of the estimation model for this particular PV system will be part of the future work.

The variations of different measured parameters during the peak for the two systems are shown in Fig. 4. While Figs. 4*b–d* show the variations of the ambient temperature, module temperature, and PPI from 2 to 4 PM, Fig. 4*d* shows the variation of PPI during the eclipse peak minute-by-minute. The module temperature and PPI for systems $\mathscr{A}$ and $\mathscr{B}$ show a strong visual correlation while the ambient temperature curves show a steeper dip for system $\mathscr{B}$ than for system $\mathscr{A}$. These visual correlations imply a strong positive relationship during the eclipse between such weather parameters of the two geographically separate PV systems. This correlation, though not an indication of dependency, is a marker of how the two PV systems can be aggregated or utilised in combination during the eclipse to address associated loads and other aspects in the future high penetration scenarios.

To further explore the relationship between irradiance, ambient temperature, and module temperature for Systems $\mathscr{A}$ and $\mathscr{B}$ (a total of six variables), bi-variate scatter plots were done for both during the eclipse duration between 2:00 and 3:00 PM as well as during eclipse peak between 2:40 and 3:00 PM, which is illustrated in Figs. 5*a* and *b*, respectively. The plots show a 6×6 matrix with the probability density function of the six variables along the primary diagonal, scatter plots with model fitting below the diagonal, and the Pearson correlation coefficient above the diagonal. The model

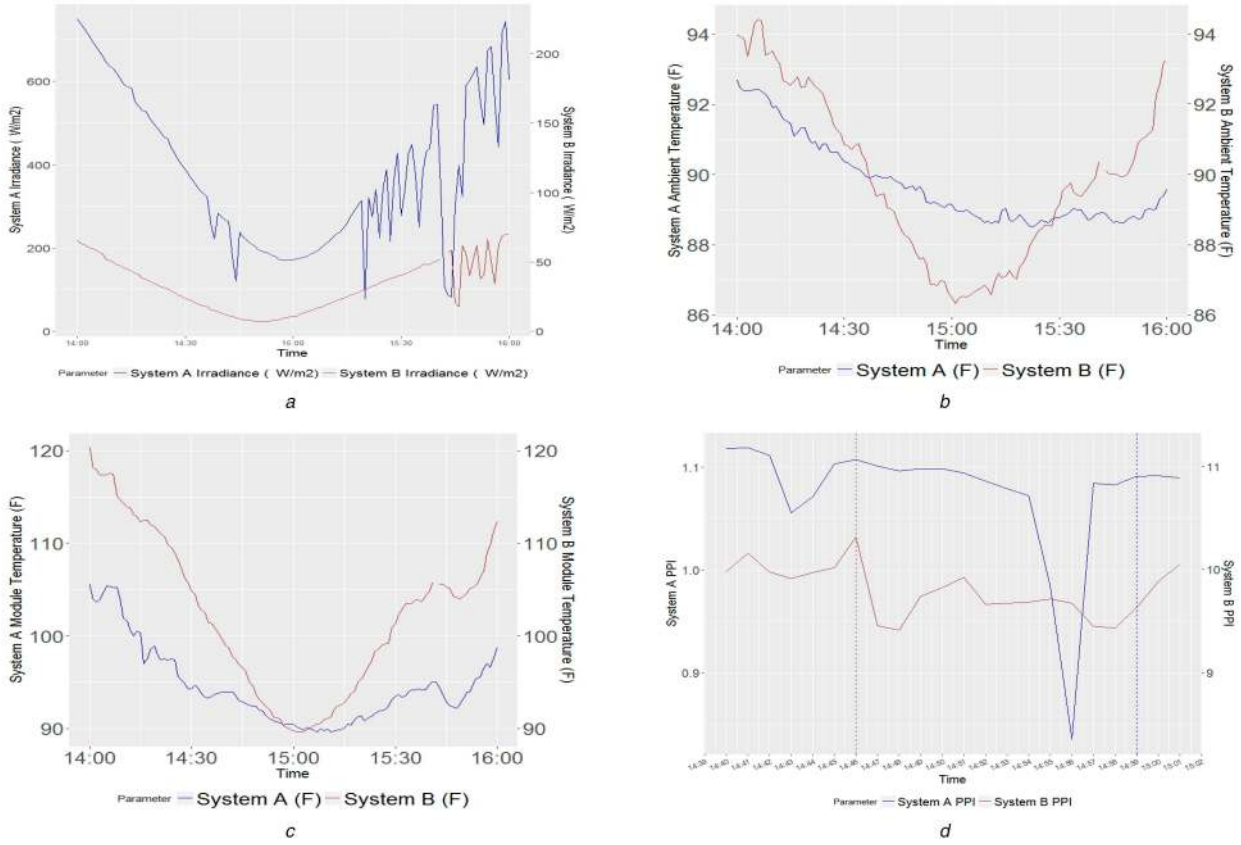

Fig. 4 *Profiles of different parameters during eclipse peak*
(a) Irradiance, ***(b)*** Ambient temperature, ***(c)*** Module temperature, ***(d)*** PPI

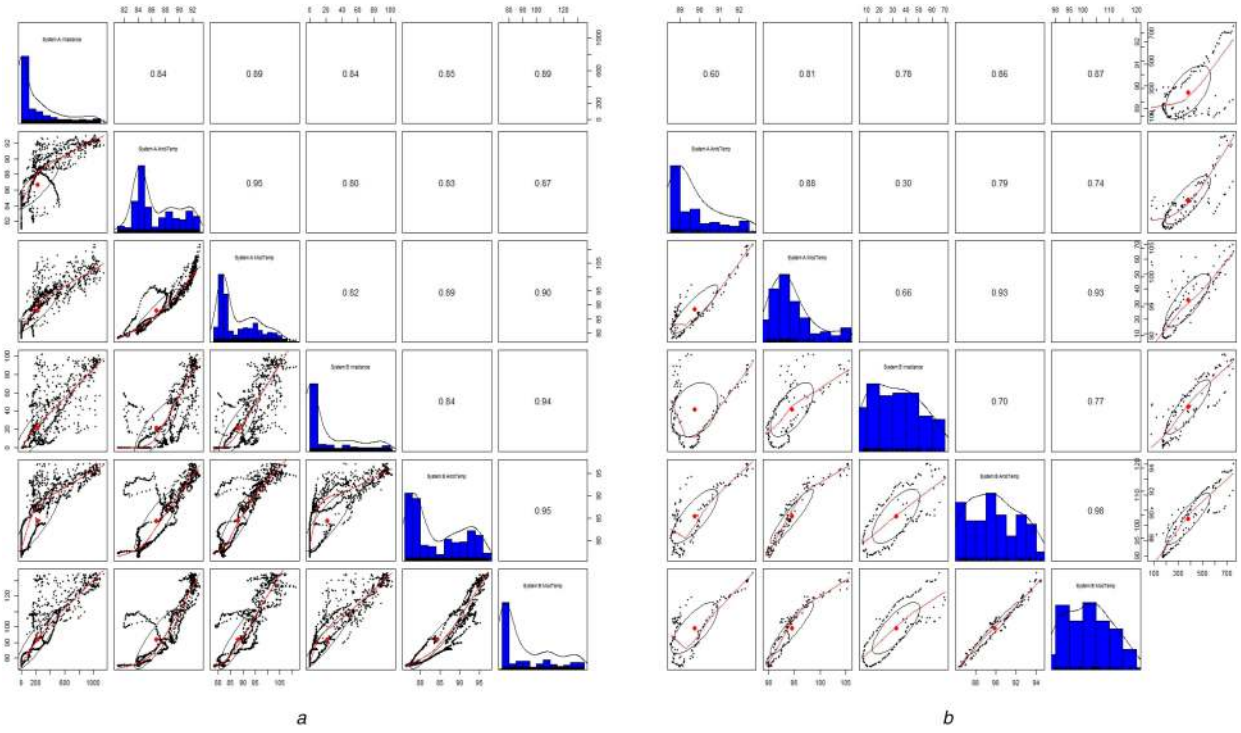

Fig. 5 *Relationship between the different weather parameters during the eclipse period and peak*
(a) Bi-variate scatter plots during the eclipse period, ***(b)*** Bi-variate scatter plots during eclipse peak

fitting shows that all of the relations between parameters within and between the systems are linear. However, this relationship changes during the eclipse peak where the ambient temperature of the system $\mathscr{A}$ has a curvilinear relationship with other parameters of both $\mathscr{A}$ and $\mathscr{B}$. Overall, the correlation coefficients of the parameters of the two systems show a drop during the eclipse peak, suggesting the two systems have a less strong positive relationship during this period, and hence could be used in aggregation-related studies. For example, the power from system $\mathscr{A}$ could be used to meet the deficit observed at system $\mathscr{B}$ provided the cost of power transfer is less than other alternatives.

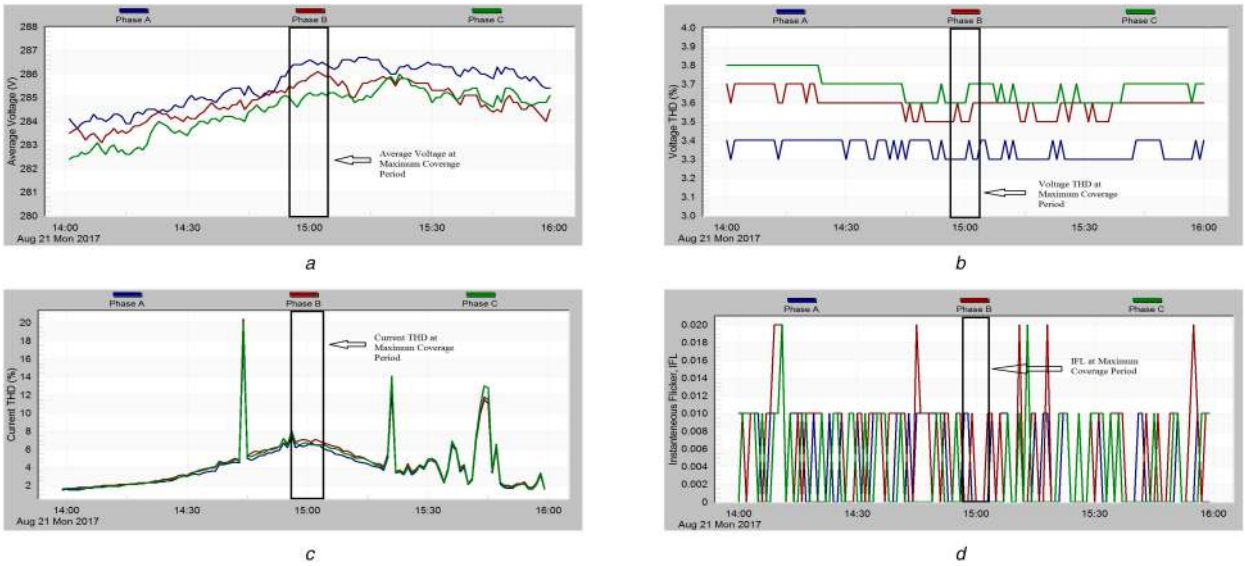

Fig. 6 *Profiles of different power quality metrics at POI during solar eclipse period of grid-tied system 𝒜*
(a) Average RMS voltage, ***(b)*** Voltage THD, ***(c)*** Current THD, ***(d)*** IFL

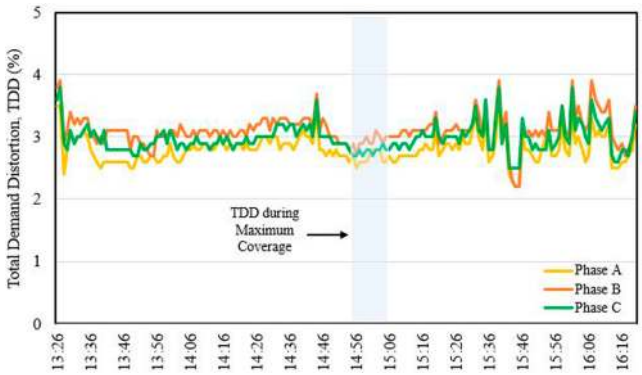

Fig. 7 *TDD during solar eclipse period*

5.2 Power quality analysis at the POI

Impacts of the eclipse on power quality metrics at the POI of system 𝒜 are analysed in the following sections. Observations on the average RMS voltage, harmonics (both voltage and current), TDD, and flicker are also discussed.

5.2.1 Average voltage: PV generation affects the feeder voltage where it is connected to. According to IEEE Standard 1547-2018, the feeder voltage at a low-voltage distribution network can vary within ±5% of the base voltage. Therefore, the minimum and maximum allowable ranges of average RMS voltage at the POI are 265 and 292 V, respectively. The average RMS voltage at the POI during the eclipse is illustrated in Fig. 6*a*. The average voltage was expected to drop at maximum coverage due to reduced generation, but an opposing trend of voltage change is observed. The system 𝒜 has a marginal impact on voltage change at the POI during the eclipse.

5.2.2 Harmonics: Current THD is expected to increase rapidly during the eclipse peak due to low solar irradiance and PV generation because THD is inversely proportional to the fundamental RMS current value of PV inverters [24, 33]. On the other hand, voltage THD should vary very little as the voltage at the POI is allowed to change in small ranges. The voltage and current THDs during the eclipse are shown in Figs. 6*b* and *c*, respectively. The measured voltage THD varies between 3.4 and 4%, which is within the IEEE Standard 1547-2018 for voltage THD (5%). A large range of current THD value (from 2 to 35%) was observed during the eclipse. Several sharp spikes were identified in Fig. 6*c* because current distortion is very sensitive to the frequent changes of incident solar radiation (caused by cloud movements) [60]. To investigate the current distortion impact of the solar eclipse, the TDD is plotted as shown in Fig. 7. The TDD curve is relatively flat during the eclipse, except for some minor fluctuations. If the PV system 𝒜 provides a larger percentage of the total demand current, the TDD effect would become prominent.

5.2.3 Flicker: Figs. 6*d* and 8*a, b* show three flicker indices during the eclipse that express small voltage variations at the POI. Both P_{st} and P_{lt} are within 1.0 and 0.8, respectively, and are within the IEEE Standard 1453-2015 voltage fluctuation limit. The variations observed in these three figures seem very small, but the scenario could be different at high penetration during the solar eclipse.

The values of different power quality parameters at the POI of system 𝒜 during the start, end, and peak of the eclipse, along with the corresponding IEEE standards limits, are presented in Table 4. It clearly indicates that the quality of power at the POI of system 𝒜 during the eclipse was within allowable IEEE standard at the existing penetration level.

5.3 Voltage regulating devices operation and analysis

The sharp ramps in irradiance and, consequently, the generation of the PV systems during an eclipse has some impacts on the voltage profile of the network, the operations of the legacy voltage control devices (VRs and OLTCs), and losses in the network. The severity of these impacts depends, among others, on the location of the POI of the systems, the penetration level of these systems, the control setting of the voltage regulation devices, the level of ramping of the power generation from the systems, and the load profile of the network.

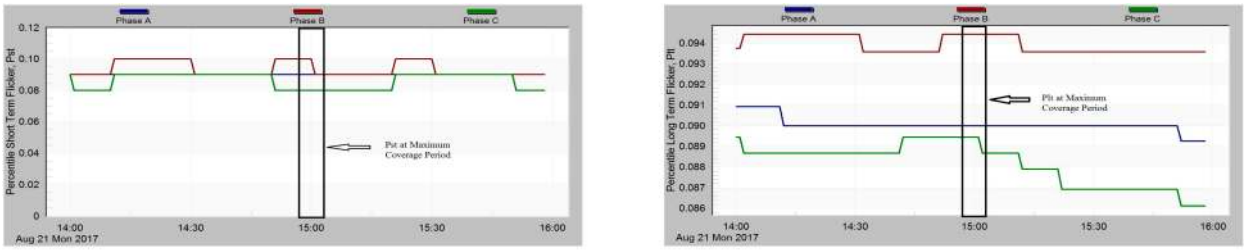

a *b*

Fig. 8 *Profiles of different power quality metrics at POI during solar eclipse period of grid-tied System 𝒜*
(a) P_{st}, ***(b)*** P_{lt}

Table 4 Power quality metrics statistics during the solar eclipse of 21 August 2017

Power quality metrics	Phase	Start time (1:26 PM)	Maximum coverage (2:58 PM)	End time (4:20 PM)	IEEE standard
average	A	283.4	286.8	284.8	265–292
RMS	B	283.1	286.0	284.4	265–292
Voltage	C	282.9	285.3	284.3	265–292
voltage THD, %	A	3.5	3.4	3.5	5.0
	B	3.7	3.6	3.7	5.0
	C	3.8	3.7	3.8	5.0
current THD, %	A	4.8	6.7	5.6	—
	B	5.1	7.5	5.7	—
	C	5.1	7.0	5.7	—
TDD	A	3.5	2.6	3.2	5.0
	B	3.8	2.9	3.5	5.0
	C	3.6	2.7	3.4	5.0
IFL	A	0.01	0.0	0.0	—
	B	0.01	0.0	0.01	—
	C	0.0	0.0	0.01	—
P_{st}	A	0.09	0.09	0.09	1.0
	B	0.09	0.1	0.09	1.0
	C	0.08	0.08	0.08	1.0
P_{lt}	A	0.091	0.09	0.089	0.8
	B	0.0945	0.0945	0.0935	0.8
	C	0.0885	0.0895	0.086	0.8

5.3.1 VR and LTC operations: The dynamic changes in the voltage profile of the network due to the ramp in power output of the PV systems cause the LTCs and VRs to tap change in other to control the voltage within the ANSI C84.1-2011 voltage standard. Fig. 9 and Fig. 10 show the various tap changing done by the VRs and the substation transformer LTC. For the feeders under study, substation transformer did not tap at all. Obviously, this is due to the relatively far distance between the PVs and the substation, and the presence of other voltage control devices close to the PVs to affect some voltage regulation. A tap change on the substation transformer is always the last resort for voltage control because a change in tap affects the whole feeder voltage downstream the network. Of the three VRs downstream the feeder, Vreg 3 tapped the most (seven times on phase A, five times on phase B and none on phase C) during the eclipse. This was due to its proximity to system 𝒜 (coupled with its relatively large size compared with system 𝒝) and Cap 0. Vreg 3 tapped three times on phase A, no tap change on phase B, and phase C during the simulated event. Vreg 4 did not tap change at all during the simulated event. This could be partly due to the voltage control action done by Cap 3.

5.3.2 Capacitors operation: During the simulated eclipse scenario, capacitors Cap 0 and Cap 3 injected reactive power into the network. Capacitors Cap 1 and 2 injected approximately zero amount of reactive power. The proximities of Cap 1 and Cap 2 to the substation and the rigidity of the grid voltage upstream the feeder could possibly explain this negligible injection of reactive power by Caps 1 and 2. The capacitor control settings of Caps 1 and 2 prevented them also from injecting power due to the relatively small variation in voltage before and during the eclipse. The downstream locations of Cap 3 and 0 coupled with their proximities to Vreg 2 and 4 and the PV systems could be responsible for their reactive power injections. The reactive power injections on phases B and C of Cap 0 is higher than that of phase A. This would explain why there was a constant tapping down on phase B and tapping up of phase A of Vreg 2. It is interesting to note the profile of the reactive power injection by Caps 0 and 3. During the eclipse time frame, the ramps (loss in power generation from the PV systems) consequently led to a reduction in the reactive power injection by the capacitors. The constant reactive power injection as seen for the first 500 min of Caps 0 and 3 was due to the relatively constant voltage of the feeder prior to power generation by the PVs.

5.3.3 Voltage profile: The feeder voltages (on the buses) plotted against their distances from the substation are as shown in Figs. 11 and Fig. 12. PV systems 𝒝 and 𝒜 are ∼3.75 and 12.5 km from the substation, respectively. The two plots (Figs. 11 and 12) show that the voltage profile at the instant when the peak of the eclipse occurred at both PV locations. At the peak of the eclipse on PV system 𝒜, the ramp down apparently had no voltage impact on the voltage profile, since as expected the ramp down in generation could only lead to a decrease in voltage at the POI. Also at this instant at PV system 𝒝, its proximity to the substation makes the voltage at the POI much more rigid, reducing the possibility of a fluctuation in voltage as a result of the eclipse. Also, from Fig. 12, the peak of the eclipse on the PV system 𝒝 did not cause any significant impact on the voltage profile on the feeder. At this instant, the power on PV system 𝒜 tends to ramp up which led to a sharp increase in voltage at the POI downstream of the feeder. The

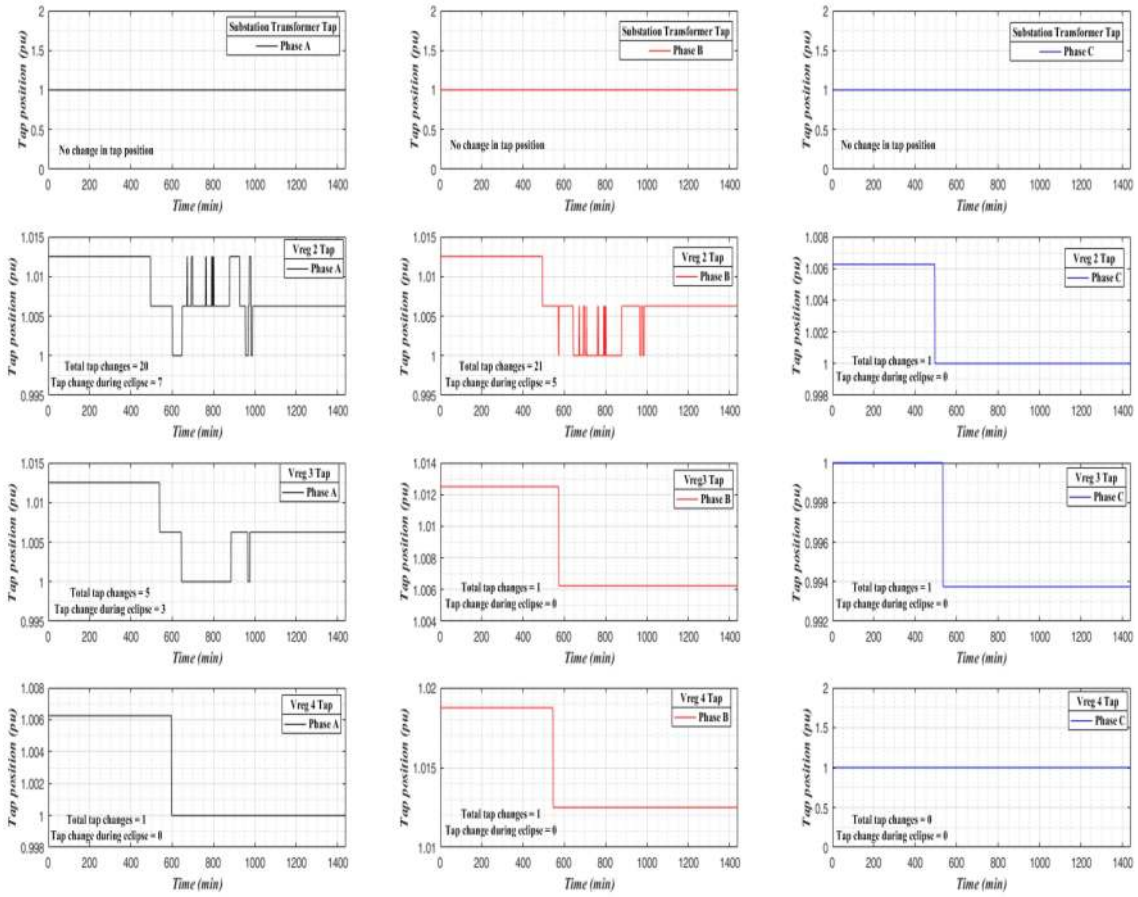

Fig. 9 *LTC and VR tap changing during the eclipse*

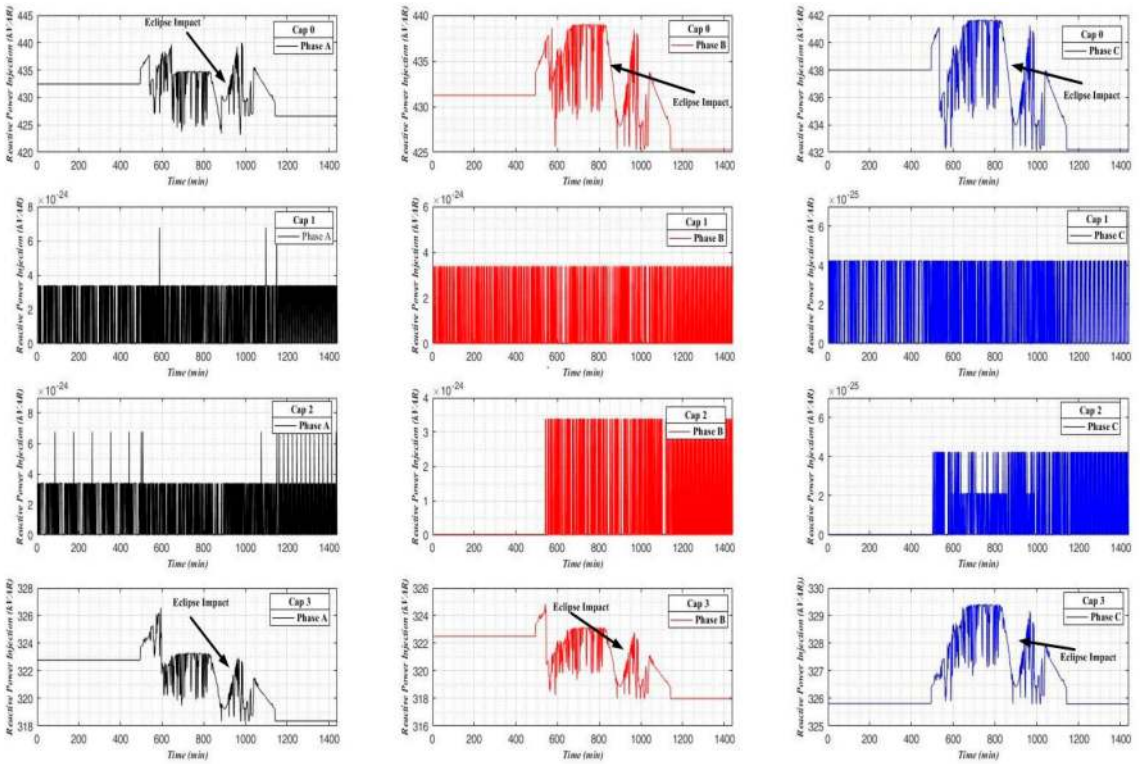

Fig. 10 *Capacitor bank reactive power injection during the eclipse*

penetration level of these systems obviously did not produce any significant impact on the voltage profile during the eclipse event. With higher levels of penetration, these impacts could become severe.

5.3.4 Network losses: The time-series plot of the overall system losses (transformer losses plus the line losses) is shown in Fig. 13. Locating PVs downstream a feeder usually reduces the overall system losses by improving the voltage profile downstream. This is quite obvious from the plot. The losses are the network starts

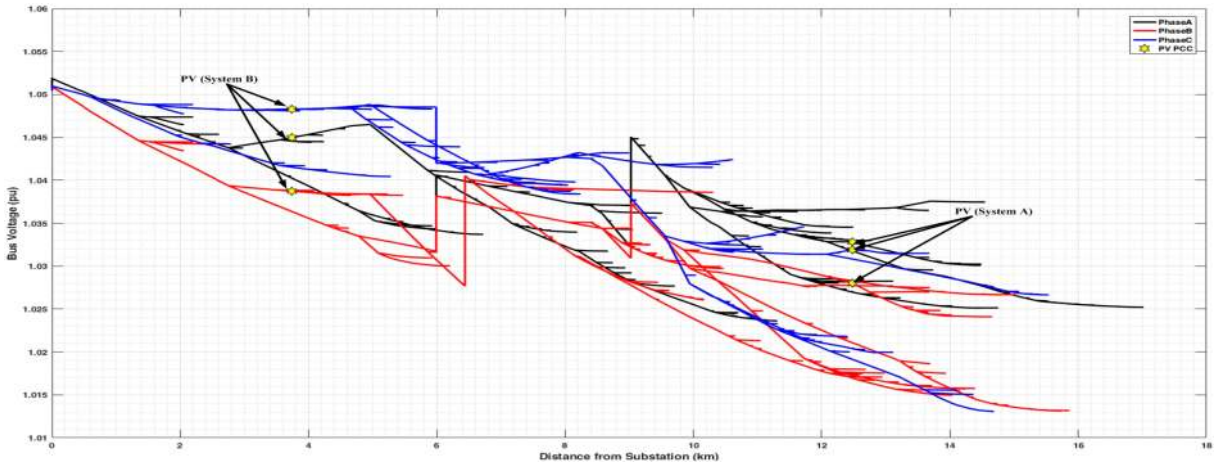

Fig. 11 *Feeder voltage profile at the peak of the eclipse on PV (system A)*

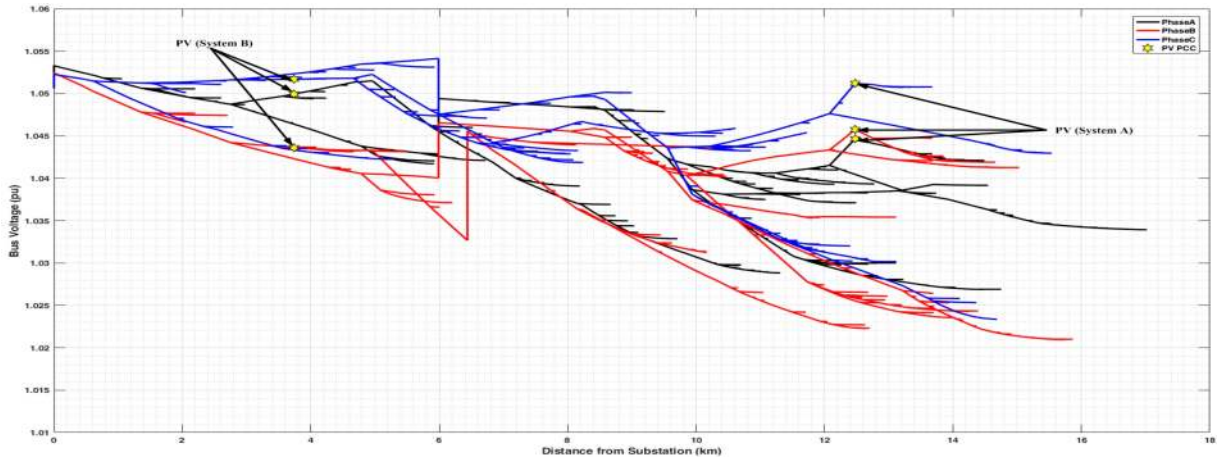

Fig. 12 *Feeder voltage profile at the peak of the eclipse on PV (system B)*

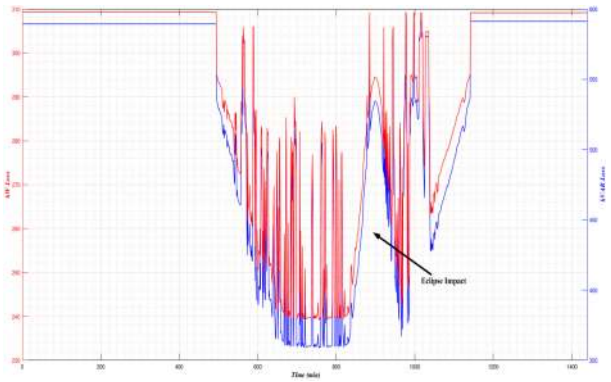

Fig. 13 *Active and reactive system losses during the eclipse*

reducing at the instant of aggregated PV generation from both PV plants. The effect of the eclipse is also seen from the loss plot. During the eclipse, the shortfall in generation from the PV led to an increase in the overall system losses during the eclipse.

5.4 Reliability analysis at the management areas

To evaluate the relationship between system reliability at the management areas and common weather parameters, the daily number of sustainable interruptions is collected from the Miami management area ranging from 1st January 2015 to 30th April 2017. The daily number of lightning strikes L is collected from the local utility's weather station centrally located at the Miami management area. The other four common weather parameters including L, W, P, and A are hourly sampled from the Miami International Airport. After data collection, both the reliability and common weather data are integrated as inputs to train the regression models defined in (15).

In the proposed MLP forecasting model, the input layer contains five types of common weather parameters and corresponding daily numbers of sustainable interruptions derived by their regression models. The MLP hidden layer is set with 20 neurones, and the output layer involves the target number of sustainable interruptions. The BP algorithm is introduced to train, validate, and test the proposed MLP forecasting model, where 70% of the collected data is used for training, 15% of the data is implemented for validating, and the remaining 15% is applied for testing. For all training, validating, and testing sections, Fig. 14 compares the target numbers of sustainable interruptions with the predicted numbers derived by the proposed MLP forecasting model [61]. In this figure, we can find that the proposed MLP forecasting model provides an acceptable result in comparison with the actual numbers of sustainable interruptions in most time periods. In particular, the proposed MLP forecasting model derives a MSE of 315.4.

In addition, the sensitivity analysis is used to evaluate the effect of each common weather parameter on the daily number of sustainable interruptions. The sensitivity value is calculated by the first-order derivative of MLP function with respect to the network parameters. Fig. 15 presents the sensitivity of each weather parameter response to the daily number of sustainable interruptions. In this figure, we can find that lightning strike L is the most important weather parameter that has an influence on the daily number of sustainable interruptions, while the average temperature T has the least impact on the daily number of sustainable interruptions. This phenomenon can be explained that most numbers of sustainable interruptions happen ranging from June to September during 1 year, which is the raining season for the Florida and lightning strikes happen most frequently. Since the average temperature of Florida almost keeps between 80 and 95°F

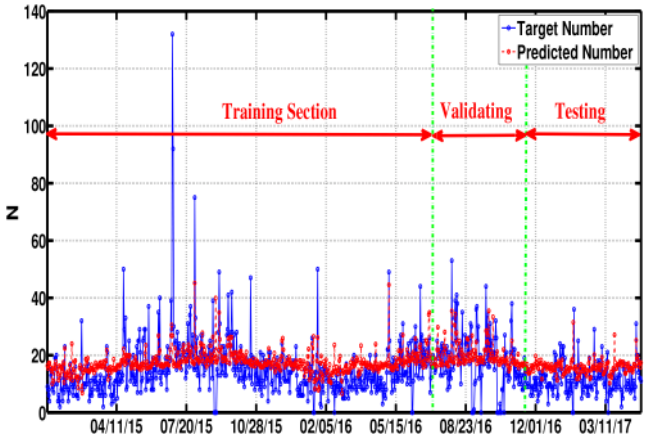

Fig. 14 *Comparison between the target numbers of sustainable interruptions and the predicted numbers derived by the proposed MLP forecasting model*

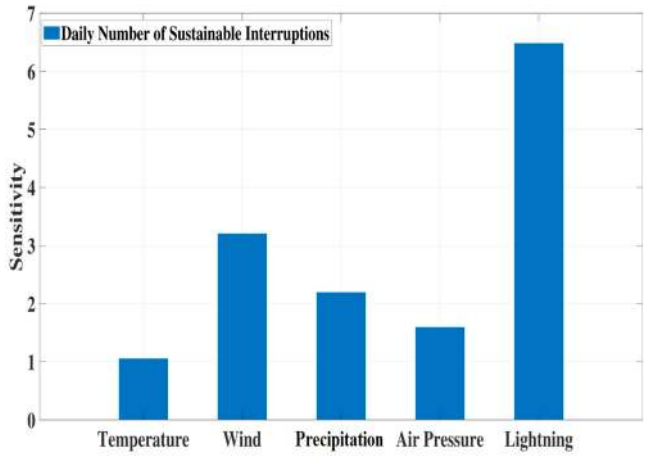

Fig. 15 *Sensitivity analysis of the daily number of sustainable interruptions with each weather parameter*

for the most months during the year, the temperature change has fewer impacts.

5.5 Comparison with existing eclipse PV impact studies

The National Renewable Energy Laboratory (NREL) conducted a pre-event analysis of the 21 August 2017 eclipse on the Western Electricity Coordinating Council [62]. The loss in a generation was estimated to be around 5.2 GW of which 4 GW loss was from utility-scale PV and the rest from the distributed PV systems. The post-event analysis based on the data collected by NREL researchers showed that loss in utility-scale PV generation was accurately predicted. There were no major impacts on the reliability and the power quality of the system. Conventional power sources such as natural gas generators and hydropower were ramped up to mitigate the impacts of the loss in generation from the PVs. The study provided some insights into how more accurate future solar eclipse impact studies can be carried out. With the increasing level of penetration, larger system-wide disturbances and impacts are expected. Also, a post 21 August 2017 eclipse study was carried out by Arzani *et al.* [63]. This paper used the solar irradiance and temperature measurements from the solar eclipse events, to simulate a real-time grid-connected utility-scale PV. The study provided some insights on the spinning reserve or sizes of storages that can be dispatched during the solar eclipse, the necessity for coordination of these PV and energy storage systems in other to maintain the system's stability as well as the importance of fast frequency control during this event. Load control methods were also discussed as effective alternative methods to address the impact of the solar eclipse event. Most of the case studies presented after the event was not at the device level. PV site performance, detailed power quality analysis, and voltage regulating device operations were not reported in details as presented in this paper.

6 Conclusion and future work

When the penetration of distributed PV systems into the smart grid increases, natural phenomena such as solar eclipse would have significant impacts on the systems and the larger grid. To demonstrate the impacts, this paper explored how the eclipse of 21 August 2017, impacted the performance of two PV systems, $\mathscr{A}$ located in Miami and $\mathscr{B}$ located in Daytona. It was observed that System $\mathscr{A}$, despite being larger in generation capacity than $\mathscr{B}$ showed a slower increase in performance during the eclipse peak owing to a slower drop in irradiance, ambient temperature, and module temperature. The steeper drop in these parameters for system $\mathscr{B}$ showed a pronounced effect in the PPI increase for it. Further statistical analysis showed a strong positive relationship between these three parameters both within and across the two systems. This relationship can be expanded to more number of systems over different geographical areas to enable aggregation studies to meet dynamic demands during such predictable events.

This paper investigated the effects of the partial solar eclipse on power quality parameters such as average RMS voltage, harmonics, and flicker at POI of system $\mathscr{A}$ and presented how those parameters vary during the eclipse period. The variability of system power indices was found to be within allowable limits in accordance with IEEE Standard. The results show that system $\mathscr{A}$ had minimum impact on power quality metrics at the current penetration level during the eclipse, but could have a severe effect at high penetration scenarios.

The impact of the eclipse on the feeder was studied by modelling the real parameters of the two feeders ($\mathscr{A}-$ and $\mathscr{B}$) as well as the PV systems ($\mathscr{A}-$ and $\mathscr{B}$) into a standard IEEE 8500 test distribution network. The simulation results showed the various impacts of the eclipse on the voltage profile as well as operations of the voltage regulation devices in the network. The VRs and the capacitor banks closest to the locations of the PV were forced to operate more frequently during the severe ramp down caused by the eclipse event. The PV system $\mathscr{B}$, which is close to the substation had little impact on the voltage profile while PV system $\mathscr{B}$ which is further downstream from the substation caused and an increase in the voltage at the POI during the eclipse event. The losses in the network were also impacted by the eclipse event. The ramping in the PV power output led to an increase in the overall system losses during the eclipse.

Finally, the impact of the eclipse at a wider, management-area level was analysed by first understanding the relationship between common weather parameters and reliability indices using the regression models. Taking the derived regression models as inputs, we proposed an MLP to forecast the daily reliability indices using time series of common weather data. In addition, we can derive the sensitivity of each common weather parameter with respect to the daily numbers of sustainable interruptions. For the utility management area in Florida, we can find that the lightning strike is the most important common weather parameter impacting on the reliability performance of the smart grid distribution networks, while the average temperature has the least impacts.

As future work, a PV generation forecasting model will be developed to explore how the utilities can predict the generation profiles of PV systems of different sizes and at penetration levels, which could help in the planning processes. Factors influencing the performance of the estimation model will also be investigated. Furthermore, additional statistical methods such as regression and dependency analysis will be conducted in addition to correlation and relationship study to explore aggregation opportunities during the eclipse to manage surges or drops in loads. This paper was done without any voltage and frequency regulation from the smart inverters. With increasing PV penetration, the use of smart inverters for voltage and frequency regulation will become inevitable. The use of the various smart inverter functionalities to address the various challenges that will be imposed during an eclipse event will be investigated. The optimal settings and coordination of these devices during these events will be analysed.

The economic consequence of the possible reduction in a life span of these legacy devices due to the increase in their switching will also be of interest to many utility companies. Finally, for the reliability analysis, other factors such as power system equipment failure rates and ageing of distribution network components will be considered in addition to the weather parameters for the regression and prediction methods discussed in this paper.

7 Acknowledgment

The material published is a result of the research supported by the National Science Foundation under the Award no. CNS-1553494.

8 References

[1] Hosenuzzaman, M., Rahim, N., Selvaraj, J., *et al.*: 'Factors affecting the PV based power generation'. 3rd IET Int. Conf. on Clean Energy and Technology (CEAT), Kuching, Malaysia, 2014, pp. 1–6, doi: 10.1049/cp.2014.1467

[2] Anzalchi, A., Sarwat, A.: 'Overview of technical specifications for grid-connected photovoltaic systems', *Energy Convers. Manage.*, 2017, **152**, pp. 312–327. Available at http://www.sciencedirect.com/science/article/pii/S0196890417308737, accessed September 2018

[3] Sarwat, A.I., Sundararajan, A., Parvez, I.: 'Trends and future directions of research for smart grid IoT sensor networks'. Proc. Int. Symp. on Sensor Networks, Systems and Security, Lakeland, Florida, August 2017, pp. 45–61

[4] California Independent System Operator.: 'Performance of ISO's system during August 21, 2017 eclipse', 2017, p. 12

[5] Uttam, A., Hongming, Z.: 'A wide-area perspective on the August 21, 2017 total solar eclipse', White Paper, April 2017

[6] Olowu, T.O., Sundararajan, A., Moghaddami, M., *et al.*: 'Future challenges and mitigation methods for high photovoltaic penetration: a survey', *Energies*, 2018, **11**, (7), pp. 1–32. Available at http://www.mdpi.com/1996-1073/11/7/1782, accessed September 2018

[7] Veda, S., Zhang, Y., Tan, J., *et al.*: 'Evaluating the impact of the 2017 solar eclipse on the U.S. western interconnection operations', U.S. Department of Energy Solar Energy Technologies Office Technical Report, 2018

[8] Peterson, Z., Coddington, M., Ding, F., *et al.*: 'An overview of distributed energy resource (DER) interconnection: current practices and emerging solutions', NREL Technical Report (number NREL/TP-6A20-72102), April 2019. Available at https://www.nrel.gov/docs/fy19osti/72102.pdf, accessed May 2019

[9] Duong, M.Q., Tran, N.T.N., Sava, G.N., *et al.*: 'The impact of 150 MWp PhoAn solar photovoltaic project into Vietnamese Quang Ngai – grid'. 2018 Int. Conf. and Exposition on Electrical and Power Engineering (EPE), Iasi, Romania, October 2018, pp. 498–502, doi: 10.1109/ICEPE.2018.8559768

[10] Sundararajan, A., Khan, T., Moghadasi, A., *et al.*: 'Survey on synchrophasor data quality and cybersecurity challenges, and evaluation of their interdependencies', *J. Mod. Power Syst. Clean Energy*, 2018, **7**, (3), pp. 1–19

[11] Sundararajan, A., Sarwat, A.I., Pons, A.: 'A survey on modality characteristics, performance evaluation metrics, and security for traditional and wearable biometric systems', *ACM Comput. Surv.*, 2019, **52**, (2), pp. 1–35

[12] Kurinec, S.K., Kucer, M., Schlein, B.: 'Monitoring a photovoltaic system during the partial solar eclipse of August 2017', *EPJ Photovolt.*, 2018, **9**, p. 7. Available at https://doi.org/10.1051/epjpv/2018005, accessed September 2018

[13] Deline, C., DiOrio, N., Jordan, D., *et al.*: 'Progress & frontiers in PV performance', *Solar Power Int.*, 2016. Available at https://www.nrel.gov/docs/fy16osti/67174.pdf, accessed September 2018

[14] Mokri, J., Cunningham, J.: 'PV system performance assessment', SunSpec Alliance and San Jose State University Technical Report, 2014. Available at https://sunspec.org/wp-content/uploads/2015/06/SunSpec-PV-System-Performance-Assessment-v2.pdf, accessed September 2018

[15] Denholm, P., Eichman, J., Margolis, R.: 'Evaluating the technical and economic performance of PV plus storage power plants', A National Renewable Energy Laboratory (NREL) Technical Report, 2017. Available at https://www.nrel.gov/docs/fy16osti/67174.pdf, accessed September 2018

[16] Kurtz, S., Riley, E., Newmiller, J., *et al.*: 'Analysis of photovoltaic system energy performance evaluation method', A National Renewable Energy Laboratory (NREL) Technical Report, 2013. Available at https://www.nrel.gov/docs/fy14osti/60628.pdf

[17] Rhee, E.: 'Not just another day of sun: reviewing the solar eclipse's effect on PV system performance', *Sol Syst. Online Article*, 2017. Available at solsystems.com/blog/2017/09/22/not-just-another-day-of-sun-reviewing-the-solar-eclipses-effect-on-pv-system/

[18] Libra, M., Kourim, P., Poulek, V.: 'Behavior of photovoltaic system during solar eclipse in Prague', *Int. J. Photoenergy*, 2016, doi: 10.1155/2016/2653560

[19] Dhople, S.V., Dominguez-Garcia, A.D.: 'Estimation of photovoltaic system reliability and performance metrics', *IEEE Trans. Power Syst.*, 2011, **27**, (1), pp. 554–563, doi: 10.1109/TPWRS.2011.2165088

[20] Kumar, B.S., Sudhakar, K.: 'Performance evaluation of 10 MW grid connected solar photovoltaic power plant in India', doi = '10.1016/j.egyr.2015.10.001', journal = Elsevier Energy Reports, 2015

[21] Haque, M.M., Wolfs, P.: 'A review of high PV penetrations in LV distribution networks: present status, impacts and mitigation measures', *Renew. Sustain. Energy Rev.*, 2016, **62**, pp. 1195–1208

[22] Ghosh, S., Rahman, S.: 'Global deployment of solar photovoltaics: ITSTS opportunities and challenges'. 2016 IEEE PES Innovative Smart Grid Technologies Conf., Europe, Ljubljana, Slovenia, October 2016, pp. 1–6

[23] Seguin, R., Woyak, J., Costyk, D., *et al.*: 'High-penetration PV integration handbook for distribution engineers', A National Renewable Energy Laboratory (NREL) Technical Report, 2016. Available at https://www.nrel.gov/docs/fy16osti/63114.pdf

[24] Chidurala, A., Saha, T.K., Mithulananthan, N., *et al.*: 'Harmonic emissions in grid connected PV systems: a case study on a large scale rooftop PV site'. 2014 IEEE PES General Meeting, Conf. & Exposition, National Harbor, USA, 2014, pp. 1–5, doi: 10.1109/PESGM.2014.6939147

[25] Thesis, A.: 'Impact of photovoltaic system penetration on the operation of voltage regulator equipment', June 2013

[26] Veda, S., Zhang, Y., Tan, J., *et al.*: 'Evaluating the impact of the 2017 solar eclipse', 2018. Available at https://www.nrel.gov/news/press/2018/nrel-researchers-measure-impact-of-eclipse-on-electrical-grid.html

[27] 'A wide-area perspective on the August 21, 2017 total solar eclipse White Paper', April 2017

[28] Panteli, M., Mancarella, P.: 'Influence of extreme weather and climate change on the resilience of power systems: impacts and possible mitigation strategies', *Electr. Power Syst. Res.*, 2015, **127**, pp. 259–270

[29] Yang, Y., Tang, W., Liu, Y., *et al.*: 'Quantitative resilience assessment for power transmission systems under typhoon weather', *IEEE Access*, 2018, **6**, pp. 40747–40756

[30] Panteli, M., Trakas, D.N., Mancarella, P., *et al.*: 'Boosting the power grid resilience to extreme weather events using defensive islanding', *IEEE Trans. Smart Grid*, 2016, **7**, (6), pp. 2913–2922, doi: 10.1109/TSG.2016.2535228

[31] Sarwat, A.I., Domijan, A., Amini, M.H., *et al.*: 'Smart grid reliability assessment utilizing boolean driven Markov process and variable weather conditions'. 2015 North American Power Symp. (NAPS), Charlotte, USA, October 2015, pp. 1–6, doi: 10.1109/NAPS.2015.7335101

[32] Sarwat, A.I., Amini, M., Domijan, A., *et al.*: 'Weather-based interruption prediction in the smart grid utilizing chronological data', *J. Mod. Power Syst. Clean Energy*, 2016, **4**, (2), pp. 308–315

[33] Anzalchi, A., Sundararajan, A., Moghadasi, A., *et al.*: 'Power quality and voltage profile analyses of high penetration grid-tied photovoltaics: a case study'. 2017 IEEE Industry Applications Society Annual Meeting, Cincinnati, USA, 2017, pp. 1–8, doi: 10.1109/IAS.2017.8101854

[34] Sundararajan, A., Sarwat, A.I.: 'Roadmap to prepare distribution grid-tied photovoltaic site data for performance monitoring'. 2017 Int. Conf. on Big Data, IoT and Data Science (BID), Pune, India, 2017, pp. 110–115, doi: 10.1109/BID.2017.8336582

[35] Anzalchi, A., Sundararajan, A., Wei, L., *et al.*: 'Future directions to the application of distributed fog computing in smart grid systems', in Information Resources Management Association (Eds.): *Cloud Security: Concepts, Methodologies, Tools, and Applications*, (IGI Global, Hershey, 2019), pp. 2186–2212

[36] Arritt, R.F., Dugan, R.C.: 'The IEEE 8500-node test feeder'. 2010 IEEE PES Transmission and Distribution, New Orleans, USA, 2010, pp. 1–6, doi: 10.1109/TDC.2010.5484381

[37] Marion, B., Adelstein, J., Boyle, K., *et al.*: 'Performance parameters for grid-connected PV systems'. Conf. Record of the Thirty-First IEEE Photovoltaic Specialists Conf., Lake Buena Vista, USA, 2005, pp. 1601–1606, doi: 10.1109/PVSC.2005.1488451

[38] Pless, S., Deru, M., Torcellini, P., *et al.*: 'Procedure for measuring and reporting the performance of photovoltaic systems in buildings', A National Renewable Energy Laboratory (NREL) Technical Report, 2005. Available at https://www.nrel.gov/docs/fy06osti/38603.pdf

[39] Haibaoui, A., Hartiti, B., Elamim, A., *et al.*: 'Performance indicators for grid-connected PV systems: a case study in Casablanca, Morocco', *IOSR J. Electr. Electron Eng. (IOSR JEEE)*, 2017, **12**, (2), pp. 55–65

[40] Townsend, T., Whitaker, C., Farmer, B., *et al.*: 'A new performance index for PV system analysis'. Proc. of 1994 IEEE 1st World Conf. on Photovoltaic Energy Conversion - WCPEC, Waikoloa, USA, 1994, pp. 1036–1039, doi: 10.1109/WCPEC.1994.520138

[41] Energy, E.: 'Guide to PV watts derate factors for enphase systems when using PV system design tools', An Enphase Energy Technical Report, 2014. Available at https://enphase.com/sites/default/files/Enphase_PVWatts_Derate_Guide_ModSolar_06-2014.pdf

[42] Yerli, B., Kaymak, M.K., Izgi, E., *et al.*: 'Effect of derating factors on photovoltaics under climatic conditions of Istanbul', *World. Acad. Sci. Eng. Technol.*, 2010, **4**, (8), pp. 1400–1404

[43] Dierauf, T., Growitz, A., Kurtz, S., *et al.*: 'Weather-corrected performance ratio', A National Renewable Energy Laboratory (NREL) Technical Report, 2013. Available at https://www.nrel.gov/docs/fy13osti/57991.pdf

[44] Bohra, R.: 'Performance analysis of 1 MW SPV plant; temperature corrected PR', *Solar Power Energy India Article*, 2014, pp. 1–4

[45] Basson, H.A., Pretorius, J.C.: 'Risk mitigation of performance ratio guarantees in commercial photovoltaic systems'. Int. Conf. Renewable Energies and Power Quality, Madrid, Spain, 2016

[46] Chaudhary, P., Rizwan, M.: 'Voltage regulation mitigation techniques in distribution system with high PV penetration: a review', *Renew. Sustain. Energy Rev.*, 2018, **82**, pp. 3279–3287. Available at http://www.sciencedirect.com/science/article/pii/S1364032117313989

[47] Hoevenaars, T., LeDoux, K., Colosino, M.: 'Interpreting IEEE STD 519 and meeting its harmonic limits in VFD applications'. IEEE Industry Applications Society 50th Annual Petroleum and Chemical Industry Conf., Houston, USA, 2003, pp. 145–150, doi: 10.1109/PCICON.2003.1242609

[48] Gutierrez, A.L.J.J., Ruiz, J., Leturiondo, L.: 'Measurement of voltage flicker: application to grid-connected wind turbines', 2010. Available at http://cdn.intechopen.com/pdfs/9948/InTech

[49] Jafari, M., Olowu, T.O., Sarwat, A.I.: 'Optimal smart inverters volt-VAR curve selection with a multi-objective volt-VAR optimization using evolutionary algorithm approach'. 2018 North American Power Symp.

(NAPS), Fargo, USA, September 2018, pp. 1–6, doi: 10.1109/NAPS.2018.8600542
[50] Olowu, T.O., Jafari, M., Sarwat, A.I.: 'A multi-objective optimization technique for volt-var control with high PV penetration using genetic algorithm'. 2018 North American Power Symp. (NAPS), Fargo, USA, September 2018, pp. 1–6, doi: 10.1109/NAPS.2018.8600557
[51] Stiles, J.: 'Voltage regulators', June 2005, pp. 8–10
[52] Manbachi, M.: 'Smart grid adaptive volt-VAR optimization in distribution networks', 2015
[53] Harrell, F.E.: '*Ordinal logistic regression*' (Springer International Publishing, Cham, 2015), pp. 311–325
[54] Wei, L., Sarwat, A.I.: 'Hybrid integration of multilayer perceptrons and parametric models for reliability forecasting in the smart grid', arXiv preprint arXiv:1810.05004, 2018
[55] Khalid, A., Sundararajan, A., Acharya, I.*, et al.*: 'Prediction of Li-ion battery state of charge using multilayer perceptron and long short-term memory models'. 2019 IEEE Transportation Electrification Conf. (ITEC), Novi, USA, 2019, to appear
[56] Glorot, X., Bengio, Y.: 'Understanding the difficulty of training deep feed-forward neural networks'. 13th Int. Conf. Artificial Intelligence and Statistics (AISTATS), Sardinia, Italy, 2010, pp. 1–8
[57] Nguyen, D., Widrow, B.: 'Improving the learning speed of 2-layer neural networks by choosing initial values of the adaptive weights'. 1990 IJCNN Int. Joint Conf. on Neural Networks, San Diego, USA, June 1990, pp. 21–26, doi: 10.1109/IJCNN.1990.137819
[58] Karlik, B., Olgac, A.V.: 'Performance analysis of various activation functions in generalized MLP architectures of neural networks', *Int. J. Artif. Intell. Expert Syst. (IJAE)*, 2011, **1**, (4), pp. 111–122
[59] Hirose, Y., Yamashita, K., Hijiya, S.: 'Back-propagation algorithm which varies the number of hidden units', *Neural Netw.*, 1991, **4**, (1), pp. 61–66
[60] Patsalides, M., Evagorou, D., Makrides, G.*, et al.*: 'The effect of solar irradiance on the power quality behaviour of grid connected photovoltaic systems'. Int. Conf. Renewable Energy and Power Quality, Sevilla, Spain, 2017, pp. 1–7
[61] Lai, Y.-C., Huang, Y.-A., Chu, H.-Y.: 'Estimation of rail capacity using regression and neural network', *Neural Comput. Appl.*, 2014, **25**, (7), pp. 2067–2077
[62] Veda, S., Zhang, Y., Tan, J.*, et al.*: 'Evaluating the impact of the 2017 solar eclipse on U.S. western interconnection operations', National Renewable Energy Lab. (NREL), Golden, CO (United States), Technical Report, 2018
[63] Arzani, N, Jayawardene, I., Arunagirinathan, P.*, et al.*: 'Impact of solar eclipse on utility grid operations'. 2018 IEEE PES/IAS Power, Africa, June 2018, pp. 1–9